ACS APPLIED MATERIALS & INTERFACES

Research Article

Cite This: ACS Appl. Mater. Interfaces 2019, 11, 28681−28689

www.acsami.org

Self-Assembled Peptide Nanofibers Display Natural Antimicrobial Peptides to Selectively Kill Bacteria without Compromising Cytocompatibility

Weike Chen,[†] Su Yang,[†] Shuxin Li,[‡] John C. Lang,[†] Chuanbin Mao,[§] Peter Kroll,[†] Liping Tang,[‡] and He Dong*[,†]

[†]Department of Chemistry & Biochemistry and [‡]Department of Bioengineering, The University of Texas at Arlington, Arlington, Texas 76019, United States

[§]Department of Chemistry and Biochemistry, Stephenson Life Sciences Research Center, University of Oklahoma, Norman, Oklahoma 73019, United States

Supporting Information

One of the major hurdles in the development of antimicrobial peptide (AMP)-based materials is their poor capacity in selectively killing bacteria without harming nearby mammalian cells. Namely, they are antimicrobial but cytotoxic. Current methods of nanoparticle-encapsulated AMPs to target bacteria selectively still have not yet overcome this hurdle. Here, we demonstrate a simple yet effective method to address this daunting challenge by associating a natural AMP with a β-sheet-forming synthetic peptide. The integrated peptides self-assembled to form a supramolecular nanofiber, resulting in the presentation of the AMP at the nanofiber−solvent interface in a precisely controlled manner. Using melittin as a model natural AMP, we found that the conformation of melittin changed dramatically when presented on the nanofiber surface, which, in turn, modulated the induced membrane permeability of the bacterial and mammalian cell membranes. Specifically, the presentation of melittin on the nanofiber restricted its hydrophobic residues, leading to a reduction of the hydrophobic interaction with lipids in the cell membranes. Compellingly, the reduced hydrophobic interaction led to a considerable decrease of melittin's induced permeability of the mammalian cell membrane than that of the bacterial cell membrane. As a result, the AMP-displaying nanofiber preferentially permeabilized and disrupted the membrane of the bacteria without compromising the mammalian cells. Such improved membrane selectivity and cytocompatibility were confirmed in a cell-based membrane localization and live−dead assay. Our new strategy holds great promise for fabricating cytocompatible antimicrobial assemblies that offer safer and more effective administration of therapeutic AMPs. These assemblies, with intrinsic antimicrobial activity and cytocompatibility, can also serve as building blocks for the construction of higher-ordered scaffolds for other biomedical applications such as tissue engineering and regenerative medicine.

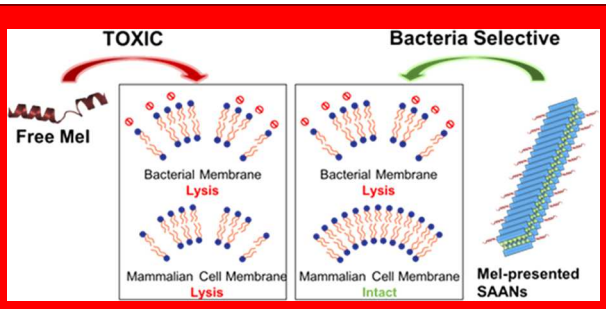

self-assembly, antimicrobial peptides, bacteria, membrane permeability, cytocompatibility

INTRODUCTION

The discovery of antimicrobial peptides (AMPs) has brought tremendous opportunities and promise to overcome the prevalence of bacterial resistance due to their action on the bacterial cell membranes that are less likely to be genetically modified.[1−4] In the past three decades, substantial efforts have been made for the development of high-throughput sources for AMP discovery; however, most AMPs have high membrane affinity and cytotoxicity against mammalian cells, which has limited their clinical applications.[5−7] To overcome the intrinsic cytotoxicity of AMPs, nanoparticles have been used as carriers for targeted delivery of AMPs to the site of infection.[8,9] However, unlike lower-molecular-weight antibiotics and anticancer drugs, the encapsulation of AMPs within a designated nanoparticulate compartment and the control over subsequent release can be challenging due to their complex secondary structures, amphiphilicity, and instability.[10−12] The construction of such multicomponent nanoparticulate formulation often requires onerous procedures. Therefore, it is highly imperative to develop simple, yet effective strategies that allow AMPs to be incorporated within a nanostructure in a precisely controlled manner while maintaining their antimicrobial activity and selectivity. The establishment of this platform technology may greatly boost the therapeutic index of AMPs, potentiating their use as clinical antimicrobials.

Supramolecular nanofibers based on the self-assembly of β-sheet-forming peptides have emerged as an important class of

Received: June 1, 2019
Accepted: July 22, 2019
Published: July 22, 2019

DOI: 10.1021/acsami.9b09583
ACS Appl. Mater. Interfaces 2019, 11, 28681−28689

biomaterials having great utility in a variety of biomedical settings.[13−18] These nanofibers, which offer unique templates for controlling the internal order and molecular packing of the therapeutics, define important parameters for effectively interfacing with cells and tissues in a controlled and predictable manner. The design and synthesis of the molecular building blocks can be highly modular by incorporating diverse functional peptides or proteins at the termini of the β-sheet-forming peptides. Upon self-assembly, nanofibers presenting multivalent ligands and epitopes can be fabricated with precisely controlled recognition sites, stoichiometry, density, and multivalency to provide desired biological functionalities. This strategy has been exquisitely applied for the construction of fibrous tissue scaffolds,[19,20] supramolecular nanofiber vaccines,[21−23] and recently angiogenic nanofibers.[24,25] However, their application for antimicrobial nanomaterial design and synthesis has rarely been explored. As most AMPs suffer from poor selectivity and severe cytotoxicity against mammalian cells, new approaches to improve their cytocompatibility are highly needed. This study will establish a new method by presenting natural AMPs on a nanofiber scaffold to improve their cytocompatibility. In addition, the self-assembly approach is highly modular with the potential of integrating multiple AMPs with distinct sequences and structures to exert synergistic effects. The preliminary results shown in this study serve as the foundation for new fundamental studies of peptide−membrane interaction in the context of a confined supramolecular framework. These results will also provide new application direction of these nanofiber scaffolds that can display a combination of various natural AMPs and potentially other biologically active peptides for a range of biomedical applications.

To fabricate these new nanofibers, we capitalized on our recent development of self-assembling antimicrobial nanofibers (SAANs) using synthetic multidomain peptides (MDPs) as the molecular building block.[26] MDPs have a general sequence of $K_x(QL)_zK_y$ (K: lysine; Q: glutamine; L: leucine) in which x, y, z represent the numbers of the repeating units of each domain. MDPs were designed to mimic natural AMPs in which a global amphiphilic β-sheet secondary structure is formed driven by the hydrophobic interaction and hydrogen bonding among the alternating $(QL)_6$ repeating units. Unlike traditional single-chain AMPs, MDPs undergo self-assembly into a sandwich-like nanofiber in which the hydrophobic leucine residues are embedded within the nanofiber. Recently, using transmission electron microscopy (TEM) and solid-state NMR, we demonstrated that partial masking of the hydrophobic surface upon self-assembly is an important factor contributing to the reduction in mammalian cytotoxicity of the MDPs, yet preserving efficacy against broad-spectrum bacteria.[27] Building on the success, we applied this self-assembly strategy to the production of cytocompatible SAANs containing natural AMPs that are known for their potent antimicrobial activity but severe cell/tissue cytotoxicity. Upon self-assembly, the constraints on the hydrophobic residues of melittin limit their hydrophobic interaction with the lipid membrane, which led to a considerably larger reduction of melittin's induced permeability of the mammalian cell membrane than that of the bacterial cell membrane. As a result, an increase in membrane selectivity toward bacteria was achieved. The results provided in the following sections serve to establish, through structural assessments, bioactivity, and biophysical evaluation of membrane response, as the next step, a SAAN-based technology platform that can be applied to a variety of naturally occurring and synthetic AMPs to improve their cytocompatibility for safer and more effective therapeutic administration.

EXPERIMENTAL SECTION

Materials. Fmoc-protected amino acids, *N,N,N′,N′*-tetramethyl-*O*-(1*H*-benzotriazol-1-yl)uronium hexafluorophosphate, 4-methylbenzhydrylamine hydrochloride salt rink amide resin were purchased from Novabiochem. Piperidine, diisopropylethylamine, 5(6)-carboxy-tetramethyl-rhodamine, Mueller−Hinton Broth (MHB), Methylthiazolyl-diphenyl-tetrazolium bromide (MTT) assay kit were purchased from Sigma-Aldrich. Solvents for peptide synthesis and purification including dimethyl formamide and acetonitrile, trifluoroacetic acid, live/dead bacterial and mammalian cell viability kit, sodium dodecyl sulfate (SDS), valinomycin, and Hoechst dye were purchased from Fisher Scientific. Dulbecco's Modified Eagle Medium (DMEM) was purchased from Life Technologies. Fetal bovine serum was purchased from VWR. TEM staining reagent, uranium acetate dihydrate, and TEM grid were purchased from TED PELLA, INC. L-α-phosphatidylglycerol (PG) (egg, chicken) (sodium salt) and L-α-phosphatidylcholine (PC) (95%) (egg, chicken) were purchased from Avanti Polar Lipids, INC. *Escherichia coli* (ATCC 25922) was purchased from ATCC.

Formulation of Mel-Integrated SAANs. Mel-containing SAANs was fabricated through co-assembly of $(QL)_6$-Mel and $(QL)_6$-K (the selection of the peptide sequences will be discussed in the section of peptide design) at various molar ratios. The two individual components were fully dissolved in a mixture of aqueous and organic solvents (typically 1:1 (V/V) water and acetonitrile) to achieve a "molecularly mixed state", followed by lyophilization and rehydration in the aqueous buffer to form water-soluble assemblies with various Mel compositions.

Circular Dichroism (CD) Spectroscopy. Samples were prepared with a total peptide concentration, namely, the sum of $(QL)_6$-K and $(QL)_6$-Mel at 50 μM in Tris buffer (pH 7.4, 20 mM). Data were collected from 250 to 190 nm at room temperature (RT) using a 1 mm cuvette, a bandwidth at 1 nm, scan rate at 100 nm/min, and a response time of 2 s. Each spectrum was averaged from three scans. The *m*Deg of rotation was converted to molar residual ellipticity via the formula $\theta = (m\text{Deg} \times 1000)/(c \times n \times l)$, where c is the concentration of the peptide solution expressed in micromolar, n is the number of amino acids in the peptide sequence, and l is the path length of the cell used in mm.

Transmission Electron Microscopy (TEM). Sample preparation was the same as that used in the CD experiment. The peptide solution (10 μL) was dropped onto a lacey carbon grid (TED PELLA 01824). After 2 min, the excess solution was carefully removed with a filter paper. The uranyl acetate aqueous solution (10 μL of 2 wt %) was dropped onto the grid for negative staining. After 2 min, the excess staining solution was removed, and the TEM samples were dried for overnight before imaging.

Minimal Inhibitory Concentration (MIC) Determination. *E. coli* was cultured in MHB media under constant shaking at 100 rpm at 37 °C to reach the midexponential growth phase. The number of bacteria was determined by counting the colony forming unit (CFU) formed on the agar plate. Bacterial suspensions were diluted to approximately 1×10^5 CFU/mL in MHB media. Peptide solutions at various total peptide concentrations (160, 80, 40, 20, 10, 5, 2.5 μM) were prepared in Tris buffer (pH 7.4, 20 mM). The peptide solution (50 μL) was mixed with 50 μL of bacterial suspension in a 96-well plate, and the experiments were performed in triplicates. The plates were incubated at 37 °C under constant shaking at 100 rpm for 18 h, and the optical density (OD) at 600 nm was measured on a plate reader. The MIC was determined as the peptide concentration in which OD reading is below 0.06, and no cloudiness was visible to naked eyes.

Membrane Permeability Assay. The preparation of PC/PG (1:1 W/W) and PC/cholesterol (8:1 W/W) liposomes followed a

DOI: 10.1021/acsami.9b09583
ACS Appl. Mater. Interfaces 2019, 11, 28681−28689

standard procedure.[28−30] Briefly, a stock liposome suspension in K^+ buffer (50 mM K_2SO_4, 25 mM HEPES−SO_4^{2-}, pH 7.2) was diluted in 1 mL of isotonic K^+ free buffer (50 mM Na_2SO_4, 25 mM HEPES−SO_4^{2-}, pH 7.2) in a glass vial. The potentiometric dye, 3,3′-dipropylthiadicarbocyanine iodide (diSC3-5), was added to reach a final concentration at 10 μM. Valinomycin was added to the suspension to reach a final concentration of 1 μM that contributes to a negative diffusion potential across the vesicles wall to quench fluorescence. The fluorescence recovery was monitored on a fluorescence spectrometer with an excitation wavelength at 620 nm and emission at 670 nm. The peptide-induced dissipation of diffusion potential was detected by the increased fluorescence intensity. The increased fluorescence intensity was converted into fluorescence recovery (F_t), defined as $F_t = [(I_t - I_0)/(I_f - I_0)] \times 100\%$, where I_t is the fluorescence intensity upon the addition of peptides at time t, I_0 is the fluorescence intensity after adding valinomycin, and I_f is the fluorescence intensity prior to the addition of valinomycin.

Mammalian Cell Membrane Localization Assay. NIH/3T3 cell suspensions were added to a confocal dish. After 24 h of incubation with peptides, the dish was washed with phosphate-buffered saline (PBS) buffer for three times to remove any nonadherent cells. DMEM cell culture media (180 μL) and 20 μL of rhodamine (Rho)-labeled peptides were added to the dish to reach a total peptide concentration at 20 μM. After 2 h of incubation, cells were washed with the PBS buffer for three times to remove any nonspecific bound peptides. Cells were stained with nuclear-specific dye, Hoechst, at room temperature for 15 min followed by PBS buffer washing for three times. Images were captured using a fluorescence microscope and processed with the ImageJ software.

RESULTS AND DISCUSSION

Design and Fabrication of AMP-Integrated SAANs. For the proof-of-concept study, we selected melittin (Mel, 26aa) as a model naturally occurring AMP, which is known to have severe cytotoxicity against mammalian cells.[31,32] Mel was conjugated to the C-terminus of an MDP with the sequence of HHHQLQLQLQLQLQL (Scheme 1). The conjugate is named as $(QL)_6$-Mel. The addition of histidine residues increases the solubility of the conjugate at the acidic pH for reverse-phase high-performance liquid chromatography (HPLC) purification. Three histidine residues were appended at the N-terminus of the $(QL)_6$ domain, whereas Mel was conjugated at its C-terminus such that Mel can exert its biological activity without potential interference from this tagging domain. Although it is not the primary focus of this study, the inclusion of histidine residues may also allow the fabrication of pH-responsive antimicrobial nanomaterials. For the second peptide, we chose a previously studied MDP (sequence: WKKQLQLQLQLQLQLKK), named as $(QL)_6$-K, which can co-assemble with $(QL)_6$-Mel to generate Mel-presenting nanofibers with controlled stoichiometry (Scheme 1).

Scheme 1. Chemical Structures of the Molecular Building Blocks for the Construction of Mel-Integrated SAANs for the Investigation of Supramolecular Structure-Dependent Membrane Selectivity and Cytotoxicity

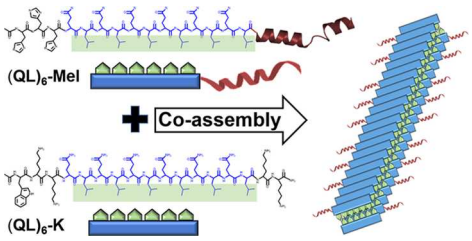

The selection of $(QL)_6$-K is based on the following considerations. First, the stability of the nanofiber is dictated by the ratio of the repeating units of each domain. Based on our previous studies, $(QL)_6$-K seemed to strike a good balance between self-assembly and disassembly, which led to highly water-soluble nanofibers with good supramolecular stability as demonstrated by the slow subunit exchange through fluorescence self-quenching.[33] Second, $(QL)_6$-K showed exceptional hemocompatibility and cytocompatibility upon nanofiber formation by confining the hydrophobic residues within the interior of the nanofiber to minimize their interaction with the cell membrane. This makes it an ideal supramolecular scaffold upon which to construct functional peptide nanostructures with good cytocompatibility. SAANs consisting of 10, 30, and 50% of Mel were formulated and characterized for their secondary structure, nanostructure, membrane selectivity, cytotoxicity, and antimicrobial activity. In the following study, they are referred to as SAANs (Mel-10%), SAANs (Mel-30%), and SAANs (Mel-50%).

Structural Characterization of the Mel-Integrated SAANs. To validate that co-assembly indeed occurred, we measured and compared the fluorescence intensity of three rhodamine (Rho)-labeled Mel-containing formulations (Figure 1a), (1) free Rho-Mel, (2) co-assembly of Rho-$(QL)_6$-Mel with $(QL)_6$-K, and (3) homoassembly of Rho-$(QL)_6$-Mel. As expected, the co-assembly exhibited fluorescence emission between the free Mel and the homoassembly of $(QL)_6$-Mel (Figure 1b), suggesting that Mel was organized within the assembly and "diluted" by $(QL)_6$-K to reduce the fluorescence self-quenching effect. The co-assembly exhibited good supramolecular stability as shown by the minimum change of the fluorescence intensity up to 24 h of incubation at room temperature (RT) (Figure S2a). A mixture consisting of free Mel and $(QL)_6$-K showed comparable fluorescence intensity to that of free Mel (Figure S2b), suggesting that no physical interaction occurred between free Mel and $(QL)_6$-K, and the co-assembly is specifically driven by the $(QL)_6$ domains. More interestingly, we found that the post-assembly product, which was formulated by mixing preformed $(QL)_6$-Mel nanofiber and $(QL)_6$-K nanofiber in the aqueous buffer, exhibited an increase of fluorescence intensity that reached a plateau after 12 h (Figure S2c). This observation further confirmed the presence of a highly specific interaction between $(QL)_6$-Mel and $(QL)_6$-K, and the co-assembly is largely driven by the consensus β-sheet-forming domain of $(QL)_6$. Notably, the final fluorescence reading of the post-assembly is lower than that of the co-assembly indicative of the presence of $(QL)_6$-Mel clusters that may self-quench, rather than being fully "dissolved" within the $(QL)_6$-K matrix (Figure S2d).

Melittin is known to adopt random coils when standing alone and changes to α-helices upon binding to the cell membrane.[32,34] The structural change was confirmed by the circular dichroism (CD) spectroscopy for free Mel in the absence and presence of sodium dodecyl sulfate (SDS) micelles, which are used to mimic the negatively charged bacterial membrane (Figure 2a). The formation of a global amphiphilic α-helix is an important factor that allows Mel to effectively interact and disrupt the bacterial cell membrane. However, due to the lack of membrane selectivity, these helical structures pose a significant challenge on the membrane integrity and cell viability of mammalian cells. Upon the

DOI: 10.1021/acsami.9b09583
ACS Appl. Mater. Interfaces 2019, 11, 28681−28689

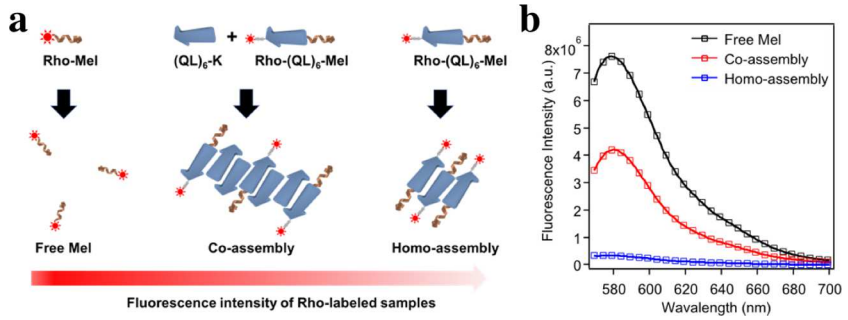

Figure 1. (a) Schematic cartoon shows the formation of Mel-integrated SAANs driven by the consensus fiber-forming domain of $(QL)_6$. Rhodamine is used as a fluorescence readout for monitoring and confirming the self-assembly and co-assembly process. (b) The fluorescence emission spectra of co-assembled Mel-presenting SAANs in comparison with free Mel and its homoassembly. Samples were prepared in Tris buffer (pH = 7.4, 20 mM) with a final concentration for free Rho-Mel at 1 μM, homoassembly of Rho-$(QL)_6$-Mel at 1 μM, and co-assembly of Rho-$(QL)_6$-Mel at 1 μM and $(QL)_6$-K at 49 μM. Spectra were acquired after 12 h of incubation at room temperature.

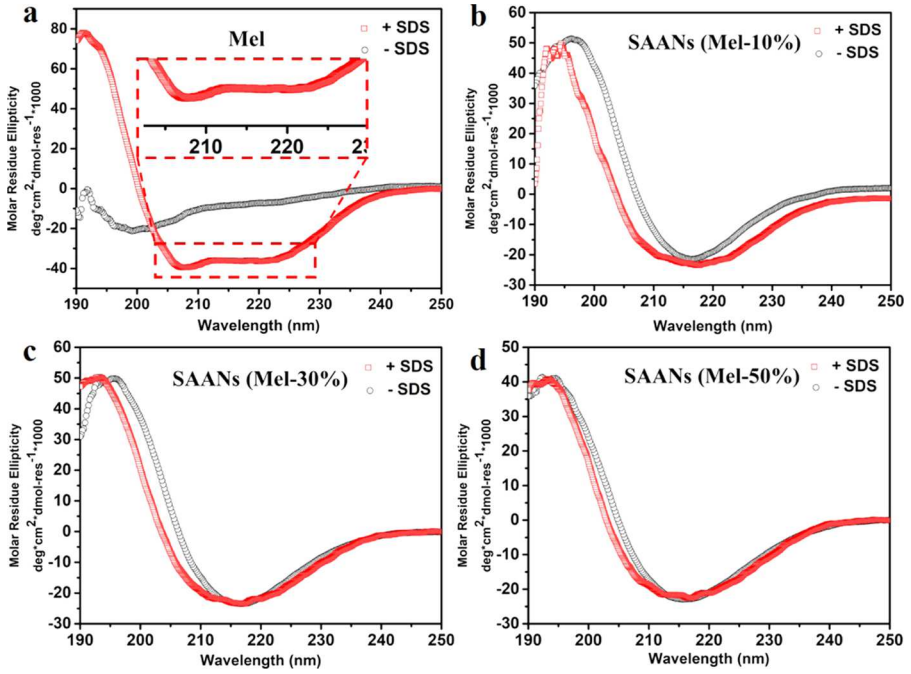

Figure 2. Secondary structures of free Mel and Mel-integrated SAANs in the absence and presence of SDS as monitored by CD spectroscopy. (a) Free Mel; (b) SAANs (Mel-10%); (c) SAANs (Mel-30%); (d) SAANs (Mel-50%). Peptides were prepared in Tris buffer (pH = 7.4, 20 mM) with a final total peptide concentration at 50 μM.

formation of SAANs, the secondary structures of Mel changed. The three co-assemblies, namely, SAANs (Mel-10%), SAANs (Mel-30%), and SAANs (Mel-50%) exhibited a typical β-sheet secondary structure with one negative absorption peak at around 216 nm in SDS-free solutions (Figure 2b–d). The Collier group reported an exquisite family of immunologically active β-sheet nanofibers, which are independent of the size and secondary structural propensity of the terminal peptide/protein antigen epitopes.[17] Inspired by these findings, we postulate that upon self-assembly, the majority of Mel was forced to form β-sheet secondary structures to accommodate the intermolecular packing of the building blocks to form supramolecular nanofibers. The structural confinement of Mel on a supramolecular scaffold was later found to be critical in modulating their membrane selectivity. In the bacterial membrane-mimicking condition (SDS micelles), small fractions of α-helices may be induced as shown by the slight shift and peak broadening toward a lower wavelength for all co-assemblies (Figure 2b–d). We are aware that CD spectroscopy may not provide a more detailed and quantitative analysis of the potential α-helical structure and its percentage. We are currently using ss-NMR spectroscopy to identify the amino acids that are responsible for the helix formation and related findings will be reported separately.

Transmission electron microscopy (TEM) was used to characterize the nanostructures of different SAANs formulation. Like most β-sheet peptide nanofibers,[35,36] all SAANs showed a polydisperse fiber length distribution. As shown in Figure 3, increasing the composition of Mel had a drastic effect on the fiber morphology, broadening the fiber diameter, and shortening the fiber length. This is presumably due to the steric hindrance caused by the bulky Mel moieties, which compromised the molecular packing of peptides in the longitudinal direction as Mel composition increases. As a control, simply mixing of free Mel with $(QL)_6$-K did not cause an appreciable change in the fiber morphology formed by

DOI: 10.1021/acsami.9b09583
ACS Appl. Mater. Interfaces 2019, 11, 28681–28689

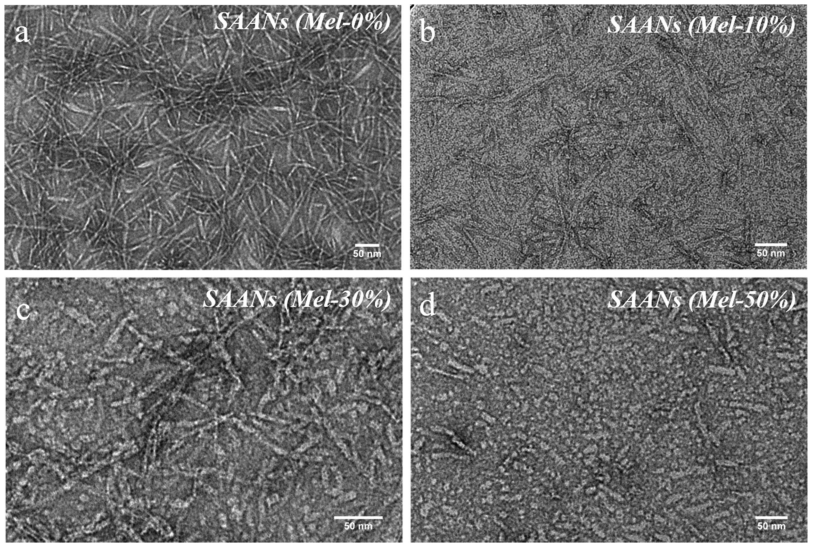

Figure 3. TEM images of SAANs containing different Mel contents. (a) SAANs (Mel-0%); (b) SAANs (Mel-10%); (c) SAANs (Mel-30%); (d) SAANs (Mel-50%). The total peptide concentration for TEM sample preparation is at 50 μM.

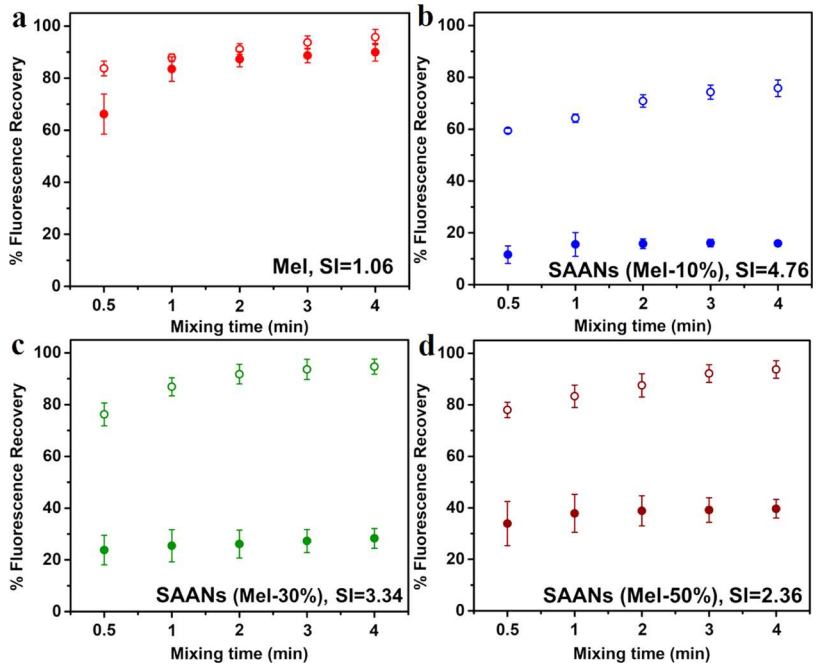

Figure 4. Membrane permeability assay by monitoring the fluorescence recovery of a membrane potential-dependent probe (diSC3-5) upon membrane disruption caused by (a) free Mel; (b) SAANs (Mel-10%); (c) SAANs (Mel-30%); (d) SAANs (Mel-50%). Open circle: PC/PG (1:1, W/W) liposomes for mimicking the bacterial membrane; Close circle: PC/cholesterol (8:1, W/W) liposome for mimicking the mammalian cell membrane. The total peptide concentration for SAANs was 20 μM. Free Mel was prepared at 6 μM.

$(QL)_6$-K (Figure S3), which suggests that physical interactions alone between free Mel and $(QL)_6$-K were inadequate for significant association or encapsulation. Integrating Mel and the β-sheet-forming $(QL)_6$ peptide is an effective means for the fabrication of Mel-integrated SAANs with tunable physicochemical properties and biological activities. Dynamic light scattering (DLS) provided a semiquantitative measurement of the volume-weighted distribution of the hydrodynamic size of different SAANs (Figure S4a), further confirming the TEM results in which the increase of Mel composition resulted in SAANs of smaller dimension. The plot of the hydrodynamic diameter by intensity (Figure S4b), more sensitive to the larger particles, showed the same trend of size reduction with the increase of Mel composition. Notably, the integration of Mel caused a wider size distribution of the nanofibers as shown by both TEM and DLS experimental results. The underlying mechanisms for such changes are of current interest and the focus of continuing systematic investigations.

Investigation of the Membrane Activity and Selectivity of Mel-Integrated SAANs. Membrane permeation assay was used to investigate the membrane activity of Mel-integrated SAANs. The basic principle of the assay relies upon the depolarization of the cytoplasmic membrane that causes fluorescence intensity change of a membrane potential-dependent probe (diSC3-5) upon membrane disruption. Liposomes with two different compositions were prepared,

DOI: 10.1021/acsami.9b09583
ACS Appl. Mater. Interfaces 2019, 11, 28681−28689

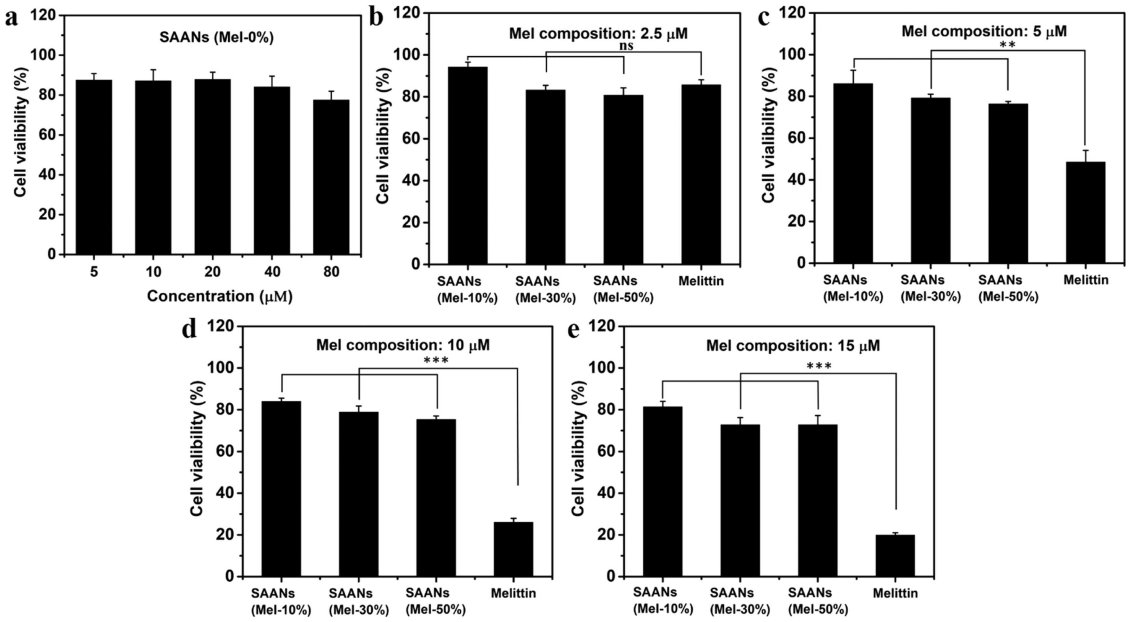

Figure 5. Cell viability assay for Mel-free SAANs, Mel-integrated SAANs, and free Mel after 24 h of incubation of peptides with NIH/3T3 mouse fibroblasts. (a) SAANs without Mel, namely, SAANs (Mel-0%) at different concentrations; (b) Mel-integrated SAANs with Mel composition at 2.5 μM; (c) Mel-integrated SAANs with Mel composition at 5 μM; (d) Mel-integrated SAANs with Mel composition at 10 μM; (e) Mel-integrated SAANs with Mel composition at 15 μM. Statistically significant differences are indicated by $^{**}p < 0.01$, $^{***}p < 0.001$, NS: not significant.

i.e., PC/PG liposomes (1:1 W/W) and PC/cholesterol liposomes (8:1 W/W) to mimic the bacterial and mammalian cell membrane, respectively.[37−39] The addition of Mel-integrated SAANs or free Mel will cause membrane disruption leading to an increase of the fluorescence intensity of diSC3-5, which was pre-encapsulated in the liposome. The fluorescence intensity can be considered as a qualitative measurement of the peptides' ability to disrupt different cell membranes. For any given sample, the bacterial/mammalian cell membrane selectivity can be quantified by the selection index (SI), which is defined and calculated as the ratio of the fluorescence intensity measured in the PC/PG liposome solution (bacterial membrane mimetics) to that of PC/cholesterol liposomes (mammalian cell membrane mimetics). As shown in Figure 4, the fluorescence recovery occurred rapidly after 30 s upon mixing liposomes with various Mel-containing samples. After reaching the equilibrium after 4 min, Mel exhibited poor membrane selectivity with a SI at 1.06, whereas the Mel-presenting SAANs dramatically improved the selectivity with SI at 4.76 for SAANs (Mel-10%), 3.34 for SAANs (Mel-30%), and 2.36 for SAANs (Mel-50%).

AMPs rely on a combined hydrophobic and electrostatic interaction to cause membrane disruption and lysis. The membrane activity of AMPs toward mammalian cells and bacteria can be adjusted by changing these interactions. The hydrophobic interaction has been considered as a more dominant factor for AMPs to permeabilize the mammalian cell membrane and cause membrane lysis compared to the bacteria.[40−42] Because of this, many studies used site-specific hydrophobic residue mutation to weaken the hydrophobic interactions of AMPs with the lipid membranes to increase the membrane selectivity.[32,43−46] In the current work, we demonstrated an alternative yet effective route to enhance the membrane selectivity of AMPs by integrating them on a supramolecular nanofiber scaffold, on which structurally confined hydrophobic residues of AMPs have limited accessibility to the lipid membrane, leading to reduced hydrophobic effects.

Cytotoxicity and Antimicrobial Activity Evaluation. The cytotoxicity is a primary concern for most natural and synthetic AMPs in clinical applications.[47] Based on the above results from membrane permeation assay, we hypothesized that structural constraint and partial shielding of Mel on SAANs may be effective to alleviate their cytotoxicity toward mammalian cells. To test the hypothesis, we performed an in vitro cytotoxicity assay for SAANs with and without Mel to free Mel in NIH/3T3 mouse fibroblasts. For the negative control group, namely, SAANs (Mel-0%), more than 80% of cell viability was observed up to 40 μM and 70% at 80 μM, suggesting good cytocompatibility of SAANs (Figure 5a). For Mel-containing SAANs, the samples were prepared to have the same Mel concentrations. Four Mel dosages at 2.5, 5, 10, and 15 μM were used for comparison of the toxicity effect from different formulations. After 24 h of incubation, MTT assay was performed to quantify the cell viability. As shown in Figure 5b−e, all three Mel-integrated SAANs demonstrated greatly reduced cytotoxicity compared to free Mel, and the difference was much more dramatic at higher Mel dosages. A more thorough dose-dependent cytotoxicity measurements were also performed (Figure S5). These results suggest that tuning the structural constraint of natural AMPs such as Mel on the nanofiber surface may be an effective route to modulate and improve their cytocompatibility. As a control experiment, we prepared a mixture consisting of free Mel and $(QL)_6$-K, which exhibited much higher cytotoxicity than that of co-assembled SAANs composed $(QL)_6$-Mel/$(QL)_6$-K (Figure S6), further supporting the important role of the local structural order and restriction for reduced cytotoxicity of Mel.

The antimicrobial activity of the co-assemblies and free Mel was investigated by (1) the minimum inhibitory concentration (MIC) assay and (2) bacterial killing efficiency assay. The MIC values were presented as both the total peptide

DOI: 10.1021/acsami.9b09583
ACS Appl. Mater. Interfaces 2019, 11, 28681−28689

concentration and the concentration of Mel in the co-assemblies (Table 1).

Table 1. MICs of Free Mel and Mel-Integrated SAANs Against *E. coli*[a]

peptides	MIC (μM)
free Mel	2.5
SAANs (Mel-10%)	>80 (8)
SAANs (Mel-30%)	10 (3.3)
SAANs (Mel-50%)	10 (5)

[a]The value in the parenthesis refers to the concentration of Mel in SAANs.

Although SAANs (Mel-10%) did not exhibit antimicrobial activity within the tested concentration range, SAANs (Mel-30%) and SAANs (Mel-50%) had MIC values (3.3 and 5 μM, respectively) that are comparable to that of free Mel (2.5 μM). The killing efficiency assay was further performed to investigate and confirm the antimicrobial activity of Mel upon integration on the nanofiber. After incubation of *E. coli* with SAANs (Mel-30%) and SAANs (Mel-50%) for 24 h, the number of bacteria was quantified by counting the colony forming units (CFU) on an agar plate. The CFU was plotted and compared with those from the control *E. coli* culture (without peptides), *E. coli* treated with SAANs (Mel-0%), and *E. coli* treated with free Mel. The results showed that both SAANs (Mel-30%) and SAANs (Mel-50%) were effective against *E. coli* growth leading to a significant reduction of bacterial numbers compared to the control *E. coli*, whereas SAANs without Mel were not effective against *E. coli* growth up to 80 μM (Figure 6). It is also not surprising that the activity of SAANs (Mel-30%) and SAANs (Mel-50%) was compromised to some degree compared to free Mel due to the partial restriction of Mel when integrated on SAANs. However, considering the reduced cytotoxicity of SAANs (Mel-30%) and SAANs (Mel-50%) (Figure 5b–e), the cell selectivity toward bacteria was dramatically improved upon the formation of SAANs.

Membrane Localization and Live–Dead Bacterial and Mammalian Cell Assay. To identify the mechanism(s) governing the reduced cytotoxicity of Mel, we investigated the cell localization of Mel-integrated SAANs upon incubation with NIH/3T3 mouse fibroblast using epi-fluorescent microscopy. For comparison, three physical mixtures of Mel/$(QL)_6$-K containing 10, 30, and 50% of Mel were prepared, and all samples were labeled with Rho for cell localization study. Cells were incubated with different peptide samples for 2 h followed by extensive washing to remove nonspecific bound peptides. As shown in Figure S7a, all physical mixtures of Mel/$(QL)_6$-K had high membrane permeability and can be found inside the cytoplasm and some even in the nucleus. Within 2 h of exposure to free Mel or Mel/$(QL)_6$-K, cells tend to shrink with a clear sign of membrane damage. In contrast, Mel-integrated SAANs were accumulated largely on the surface of the cell membrane (Figure S7b) causing negligible change on the cell membrane and overall morphology.

The live/dead assay was performed to further confirm the effect of self-assembly on Mel's cytocompatibility and antimicrobial activity. Based on the membrane permeability, MIC, and cytotoxicity assay results, we selected SAANs (Mel-30%) to perform the live/dead assay against both *E. coli* and NIH/3T3 mouse fibroblasts. Free Mel was used as a control. As shown in Figure 7a,b, a large fraction of dead *E. coli* was observed for both SAANs (Mel-30%) and free Mel (top panel)-treated bacteria culture, as shown by the red staining of propidium iodide (PI). PI was commonly used to evaluate the bacterial cell membrane integrity by penetrating bacteria, which are having damaged membranes.[48,49] This result illustrated that SAANs (Mel-30%) shared the same antimicrobial mechanism to kill bacteria through punching holes and, thus, increasing PI's permeability on the bacterial membrane. Using the live/dead fluorescence images, the cell viability was quantified showing comparable killing efficiency between free Mel and SAANs (Mel-30%) (Figure 7e). For NIH/3T3 mouse fibroblasts, although Mel still caused significant cell death as shown by the red fluorescence (Figure 7c), SAANs (Mel-30%) had dramatically reduced cytotoxicity as shown by the predominant green fluorescence from the live cells (Figure 7d). Quantitative analysis of NIH/3T3 cell viability showed much higher cell survival rates upon treatment with SAANs (Mel-30%) than those with free Mel (Figure 7f).

Although further studies are needed to fully uncover the mechanism of reduced membrane penetration and cytotoxicity, we believe that the structural constraint and partial shielding of natural AMPs play important roles in such reactions. In addition, the difference of the membrane composition and mechanics between bacteria and mammalian cells could play critical roles in mediating their interactions with AMPs that are confined in a rigid supramolecular backbone. Deeper insights are expected through detailed investigation of various lipid-associated peptide self-assemblies using ss-NMR spectroscopy.

CONCLUSIONS

Mel-integrated SAANs were fabricated to possess greatly improved membrane selectivity and cytocompatibility. By

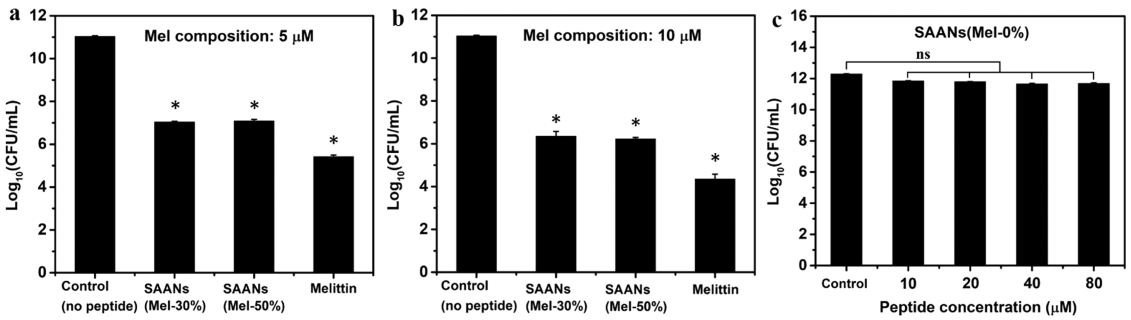

Figure 6. Numbers of *E. coli.* upon 24 h of incubation of *E. coli* with free Mel and Mel-integrated SAANs at Mel concentrations of (a) 5 μM and (b) 10 μM, (c) SAANs (Mel-0%). Statistically significant differences are indicated by $^*p < 0.05$, NS: not significant.

DOI: 10.1021/acsami.9b09583
ACS Appl. Mater. Interfaces 2019, 11, 28681–28689

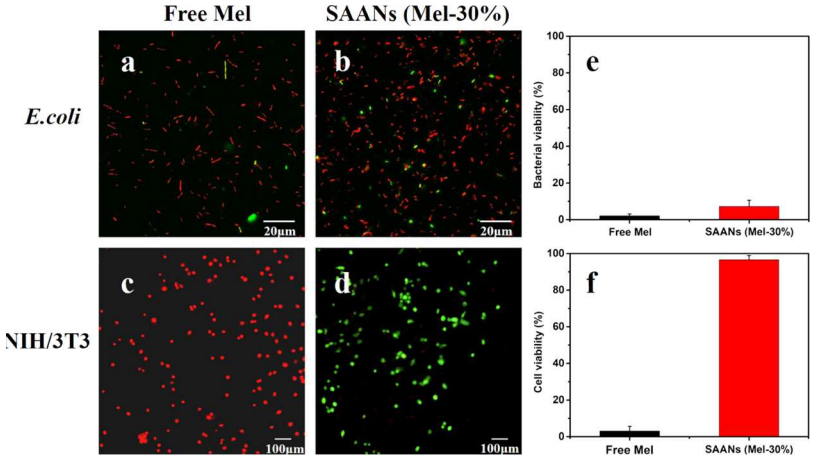

Figure 7. Merged fluorescence images of live/dead bacterial and mammalian cell assay for (a) free Mel against *E. coli*; (b) SAANs (Mel-30%) against *E. coli*; (c) free Mel against NIH/3T3 fibroblasts; and (d) SAANs (Mel-30%) against NIH/3T3 fibroblasts. (e) Quantification of *E. coli* viability and (f) NIH/3T3 fibroblast viability upon incubation with free Mel and SAANs (Mel-30%). The total peptide concentration of SAANs (Mel-30%) is 20 μM. The concentration of free Mel: 6 μM.

confining AMPs within a conformationally rigid supramolecular polymer scaffold, this new approach is found to limit AMP's flexibility and to reduce their cytotoxicity toward mammalian cells. Due to the modularity nature of the MDP assembly, the proposed system could be used to integrate multiple sequences and structurally distinct AMPs in one nanofiber entity to further enhance the antimicrobial activity against resistant bacteria through synergy. This methodology can also serve as a generic strategy for the re-engineering and reformatting of thousands of natural and synthetic AMPs available in the peptide databank as cytocompatible antimicrobials, thereby greatly boosting their therapeutic potential.

■ ASSOCIATED CONTENT

Supporting Information

The Supporting Information is available free of charge on the ACS Publications website at DOI: 10.1021/acsami.9b09583.

Experimental methods; HPLC and MALDI data; fluorescence; DLS and TEM for structural characterization; cell viability and cell localization of different SAANs formulation (PDF)

■ AUTHOR INFORMATION

Corresponding Author

*E-mail: he.dong@uta.edu.

ORCID

Chuanbin Mao: 0000-0002-8142-3659

Peter Kroll: 0000-0003-4782-2805

He Dong: 0000-0002-8494-0475

Author Contributions

All of the authors have given approval to the final version of the manuscript.

Notes

The authors declare no competing financial interest.

■ ACKNOWLEDGMENTS

This study was supported by the National Science Foundation (DMR 1824614) and the start-up funds from the University of Texas at Arlington. We thank Dr. Cara Boutte for the kind help and discussion on the bacterial imaging experiment.

■ REFERENCES

(1) Brooks, B. D.; Brooks, A. E. Therapeutic Strategies to Combat Antibiotic Resistance. *Adv. Drug Delivery Rev.* **2014**, *78*, 14−27.

(2) Hancock, R. E.; Sahl, H.-G. Antimicrobial and Host-Defense Peptides as New Anti-Infective Therapeutic Strategies. *Nat. Biotechnol.* **2006**, *24*, 1551−1557.

(3) Hassan, M.; Kjos, M.; Nes, I.; Diep, D.; Lotfipour, F. Natural Antimicrobial Peptides from Bacteria: Characteristics and Potential Applications to Fight against Antibiotic Resistance. *J. Appl. Microbiol.* **2012**, *113*, 723−736.

(4) Mahlapuu, M.; Håkansson, J.; Ringstad, L.; Björn, C., Antimicrobial Peptides: An Emerging Category of Therapeutic Agents. *Front. Cell. Infect. Microbiol.* **2016**, *6*. DOI: 10.3389/fcimb.2016.00194

(5) Kang, S.-J.; Park, S. J.; Mishig-Ochir, T.; Lee, B.-J. Antimicrobial Peptides: Therapeutic Potentials. *Expert Rev. Anti-Infect. Ther.* **2014**, *12*, 1477−1486.

(6) Yeung, A. T.; Gellatly, S. L.; Hancock, R. E. Multifunctional Cationic Host Defence Peptides and Their Clinical Applications. *Cell. Mol. Life Sci.* **2011**, *68*, 2161−2176.

(7) Marr, A. K.; Gooderham, W. J.; Hancock, R. E. W. Antibacterial Peptides for Therapeutic Use: Obstacles and Realistic Outlook. *Curr. Opin. Pharmacol.* **2006**, *6*, 468−472.

(8) Nordström, R.; Malmsten, M. Delivery Systems for Antimicrobial Peptides. *Adv. Colloid Interface Sci.* **2017**, *242*, 17−34.

(9) Piras, A. M.; Maisetta, G.; Sandreschi, S.; Gazzarri, M.; Bartoli, C.; Grassi, L.; Esin, S.; Chiellini, F.; Batoni, G. Chitosan Nanoparticles Loaded with the Antimicrobial Peptide Temporin B Exert a Long-Term Antibacterial Activity in Vitro against Clinical Isolates of *Staphylococcus Epidermidis*. *Front. Microbiol.* **2015**, *6*, 372.

(10) Biswaro, L. S.; da Costa Sousa, M. G.; Rezende, T. M. B.; Dias, S. C.; Franco, O. L. Antimicrobial Peptides and Nanotechnology, Recent Advances and Challenges. *Front. Microbiol.* **2018**, *9*, No. 855.

(11) Gallarate, M.; Battaglia, L.; Peira, E.; Trotta, M. Peptide-Loaded Solid Lipid Nanoparticles Prepared through Coacervation Technique. *Int. J. Chem. Eng.* **2011**, *2011*, No. 132435.

(12) Mohammadi-Samani, S.; Taghipour, B. Plga Micro and Nanoparticles in Delivery of Peptides and Proteins; Problems and Approaches. *Pharm. Dev. Technol.* **2015**, *20*, 385−393.

(13) Moore, A. N.; Hartgerink, J. D. Self-Assembling Multidomain Peptide Nanofibers for Delivery of Bioactive Molecules and Tissue Regeneration. *Acc. Chem. Res.* **2017**, *50*, 714−722.

(14) Acar, H.; Srivastava, S.; Chung, E. J.; Schnorenberg, M. R.; Barrett, J. C.; LaBelle, J. L.; Tirrell, M. Self-Assembling Peptide-Based Building Blocks in Medical Applications. *Adv. Drug Delivery Rev.* **2017**, *110*−*111*, 65−79.

(15) Cui, H.; Webber, M. J.; Stupp, S. I. Self-Assembly of Peptide Amphiphiles: From Molecules to Nanostructures to Biomaterials. *Biopolymers* **2010**, *94*, 1−18.
(16) Haines-Butterick, L.; Rajagopal, K.; Branco, M.; Salick, D.; Rughani, R.; Pilarz, M.; Lamm, M. S.; Pochan, D. J.; Schneider, J. P. Controlling Hydrogelation Kinetics by Peptide Design for Three-Dimensional Encapsulation and Injectable Delivery of Cells. *Proc. Natl. Acad. Sci. U.S.A.* **2007**, *104*, 7791−7796.
(17) Hudalla, G. A.; Sun, T.; Gasiorowski, J. Z.; Han, H.; Tian, Y. F.; Chong, A. S.; Collier, J. H. Gradated Assembly of Multiple Proteins into Supramolecular Nanomaterials. *Nat. Mater.* **2014**, *13*, 829−836.
(18) Bowerman, C. J.; Nilsson, B. L. Review Self-Assembly of Amphipathic β-Sheet Peptides: Insights and Applications. *Biopolymers* **2012**, *98*, 169−184.
(19) Galler, K. M.; Aulisa, L.; Regan, K. R.; D'Souza, R. N.; Hartgerink, J. D. Self-Assembling Multidomain Peptide Hydrogels: Designed Susceptibility to Enzymatic Cleavage Allows Enhanced Cell Migration and Spreading. *J. Am. Chem. Soc.* **2010**, *132*, 3217−3223.
(20) Liu, X.; Wang, X.; Horii, A.; Wang, X.; Qiao, L.; Zhang, S.; Cui, F.-Z. In Vivo Studies on Angiogenic Activity of Two Designer Self-Assembling Peptide Scaffold Hydrogels in the Chicken Embryo Chorioallantoic Membrane. *Nanoscale* **2012**, *4*, 2720−2727.
(21) Rudra, J. S.; Tian, Y. F.; Jung, J. P.; Collier, J. H. A Self-Assembling Peptide Acting as an Immune Adjuvant. *Proc. Natl. Acad. Sci. U.S.A.* **2010**, *107*, 622−627.
(22) Hudalla, G. A.; Modica, J. A.; Tian, Y. F.; Rudra, J. S.; Chong, A. S.; Sun, T.; Mrksich, M.; Collier, J. H. A Self-Adjuvanting Supramolecular Vaccine Carrying a Folded Protein Antigen. *Adv. Healthcare Mater.* **2013**, *2*, 1114−1119.
(23) Wen, Y.; Collier, J. H. Supramolecular Peptide Vaccines: Tuning Adaptive Immunity. *Curr. Opin. Immunol.* **2015**, *35*, 73−79.
(24) Wickremasinghe, N. C.; Kumar, V. A.; Shi, S.; Hartgerink, J. D. Controlled Angiogenesis in Peptide Nanofiber Composite Hydrogels. *ACS Biomater. Sci. Eng.* **2015**, *1*, 845−854.
(25) Kumar, V. A.; Taylor, N. L.; Shi, S.; Wang, B. K.; Jalan, A. A.; Kang, M. K.; Wickremasinghe, N. C.; Hartgerink, J. D. Highly Angiogenic Peptide Nanofibers. *ACS Nano* **2015**, *9*, 860−868.
(26) Xu, D.; Jiang, L.; Singh, A.; Dustin, D.; Yang, M.; Liu, L.; Lund, R.; Sellati, T. J.; Dong, H. Designed Supramolecular Filamentous Peptides: Balance of Nanostructure, Cytotoxicity and Antimicrobial Activity. *Chem. Commun.* **2015**, *51*, 1289−1292.
(27) Xu, D.; Chen, W.; Tobin-Miyaji, Y. J.; Sturge, C. R.; Yang, S.; Elmore, B.; Singh, A.; Pybus, C.; Greenberg, D. E.; Sellati, T. J.; Qiang, W.; Dong, H. Fabrication and Microscopic and Spectroscopic Characterization of Cytocompatible Self-Assembling Antimicrobial Nanofibers. *ACS Infect. Dis.* **2018**, *4*, 1327−1335.
(28) Loew, L. M.; Rosenberg, I.; Bridge, M.; Gitler, C. Diffusion Potential Cascade. Convenient Detection of Transferable Membrane Pores. *Biochemistry* **1983**, *22*, 837−844.
(29) Sims, P. J.; Waggoner, A. S.; Wang, C.-H.; Hoffman, J. F. Studies on the Mechanism by Which Cyanine Dyes Measure Membrane Potential in Red Blood Cells and Phosphatidylcholine Vesicles. *Biochemistry* **1974**, *13*, 3315−3330.
(30) Ghosh, J. K.; Ovadia, M.; Shai, Y. A Leucine Zipper Motif in the Ectodomain of Sendai Virus Fusion Protein Assembles in Solution and in Membranes and Specifically Binds Biologically-Active Peptides and the Virus. *Biochemistry* **1997**, *36*, 15451−15462.
(31) Terwilliger, T. C.; Weissman, L.; Eisenberg, D. The Structure of Melittin in the Form I Crystals and Its Implication for Melittin's Lytic and Surface Activities. *Biophys. J.* **1982**, *37*, 353−361.
(32) Asthana, N.; Yadav, S. P.; Ghosh, J. K. Dissection of Antibacterial and Toxic Activity of Melittin a Leucine Zipper Motif Plays a Crucial Role in Determining Its Hemolytic Activity but Not Antibacterial Activity. *J. Biol. Chem.* **2004**, *279*, 55042−55050.
(33) Yang, M.; Xu, D.; Jiang, L.; Zhang, L.; Dustin, D.; Lund, R.; Liu, L.; Dong, H. Filamentous Supramolecular Peptide−Drug Conjugates as Highly Efficient Drug Delivery Vehicles. *Chem. Commun.* **2014**, *50*, 4827−4830.
(34) Sui, S.-F.; Wu, H.; Guo, Y.; Chen, K.-S. Conformational Changes of Melittin Upon Insertion into Phospholipid Monolayer and Vesicle1. *J. Biochem.* **1994**, *116*, 482−487.
(35) Cormier, A. R.; Pang, X.; Zimmerman, M. I.; Zhou, H.-X.; Paravastu, A. K. Molecular Structure of Rada16-I Designer Self-Assembling Peptide Nanofibers. *ACS Nano* **2013**, *7*, 7562−7572.
(36) Dong, H.; Paramonov, S. E.; Aulisa, L.; Bakota, E. L.; Hartgerink, J. D. Self-Assembly of Multidomain Peptides: Balancing Molecular Frustration Controls Conformation and Nanostructure. *J. Am. Chem. Soc.* **2007**, *129*, 12468−12472.
(37) Lee, J.; Park, C.; Park, S.-C.; Woo, E.-R.; Park, Y.; Hahm, K. S.; Lee, D. G. Cell Selectivity-Membrane Phospholipids Relationship of the Antimicrobial Effects Shown by Pleurocidin Enantiomeric Peptides. *J. Pept. Sci.* **2009**, *15*, 601−606.
(38) Zhang, L.; Rozek, A.; Hancock, R. E. Interaction of Cationic Antimicrobial Peptides with Model Membranes. *J. Biol. Chem.* **2001**, *276*, 35714−35722.
(39) Oren, Z.; Lerman, J. C.; Gudmundsson, G. H.; Agerberth, B.; Shai, Y. Structure and Organization of the Human Antimicrobial Peptide LL-37 in Phospholipid Membranes: Relevance to the Molecular Basis for Its Non-Cell-Selective Activity. *Biochem. J.* **1999**, *341*, 501−513.
(40) Oren, Z.; Hong, J.; Shai, Y. A Repertoire of Novel Antibacterial Diastereomeric Peptides with Selective Cytolytic Activity. *J. Biol. Chem.* **1997**, *272*, 14643−14649.
(41) Toke, O. Antimicrobial Peptides: New Candidates in the Fight against Bacterial Infections. *Biopolymers* **2005**, *80*, 717−735.
(42) Glukhov, E.; Stark, M.; Burrows, L. L.; Deber, C. M. Basis for Selectivity of Cationic Antimicrobial Peptides for Bacterial Versus Mammalian Membranes. *J. Biol. Chem.* **2005**, *280*, 33960−33967.
(43) Kamech, N.; Vukičević, D.; Ladram, A.; Piesse, C.; Vasseur, J.; Bojović, V.; Simunić, J.; Juretić, D. Improving the Selectivity of Antimicrobial Peptides from Anuran Skin. *J. Chem. Inf. Model.* **2012**, *52*, 3341−3351.
(44) Hollmann, A.; Martínez, M.; Noguera, M. E.; Augusto, M. T.; Disalvo, A.; Santos, N. C.; Semorile, L.; Maffía, P. C. Role of Amphipathicity and Hydrophobicity in the Balance between Hemolysis and Peptide−Membrane Interactions of Three Related Antimicrobial Peptides. *Colloids Surf., B* **2016**, *141*, 528−536.
(45) Blondelle, S. E.; Houghten, R. A. Hemolytic and Antimicrobial Activities of the Twenty-Four Individual Omission Analogs of Melittin. *Biochemistry* **1991**, *30*, 4671−4678.
(46) Meng, H.; Kumar, K. Antimicrobial Activity and Protease Stability of Peptides Containing Fluorinated Amino Acids. *J. Am. Chem. Soc.* **2007**, *129*, 15615−15622.
(47) Aoki, W.; Kuroda, K.; Ueda, M. Next Generation of Antimicrobial Peptides as Molecular Targeted Medicines. *J. Biosci. Bioeng.* **2012**, *114*, 365−370.
(48) Gabriel, G. J.; Madkour, A. E.; Dabkowski, J. M.; Nelson, C. F.; Nüsslein, K.; Tew, G. N. Synthetic Mimic of Antimicrobial Peptide with Nonmembrane-Disrupting Antibacterial Properties. *Biomacromolecules* **2008**, *9*, 2980−2983.
(49) Lv, Y.; Wang, J.; Gao, H.; Wang, Z.; Dong, N.; Ma, Q.; Shan, A. Antimicrobial Properties and Membrane-Active Mechanism of a Potential α-Helical Antimicrobial Derived from Cathelicidin Pmap-36. *PLoS One* **2014**, *9*, No. e86364.

DOI: 10.1021/acsami.9b09583
ACS Appl. Mater. Interfaces 2019, 11, 28681−28689